

**Effect of coronal temperature  
on the scale of solar chromospheric jets**

H. Iijima and T. Yokoyama

Department of Earth and Planetary Science, The University of Tokyo, 7-3-1 Hongo,  
Bunkyo-ku, Tokyo 113-0033, Japan.

`h.iijima@eps.s.u-tokyo.ac.jp`

Received \_\_\_\_\_; accepted \_\_\_\_\_

## ABSTRACT

We investigate the effect of coronal temperature on the formation process of solar chromospheric jets using two-dimensional magnetohydrodynamic simulations of the region from the upper convection zone to the lower corona. We develop a new radiative magnetohydrodynamic code for the dynamic modeling of the solar atmosphere, employing a LTE equation of state, optically thick radiative loss in the photosphere, optically thin radiative loss in the chromosphere and the corona, and thermal conduction along the magnetic field lines. Many chromospheric jets are produced in the simulations by shock waves passing through the transition region. We find that these jets are projected farther outward when the coronal temperature is lower (similar to that in coronal holes) and shorter when the coronal temperature is higher (similar to that in active regions). When the coronal temperature is high, the deceleration of the chromospheric jets is consistent with the model in which deceleration is determined by the periodic chromospheric shock waves. However, when the coronal temperature is low, the gravitational deceleration becomes more important and the chromospheric jets approach ballistic motion.

*Subject headings:* magnetic fields — magnetohydrodynamics — Sun: atmosphere — Sun: chromosphere — Sun: transition region

## 1. Introduction

Various chromospheric jets are observed in the solar atmosphere. In quiet regions and coronal holes, we observe classical (type I) spicules at the limb, which have maximum lengths of 4–10 Mm, lifetimes of 1–7 min, and maximum upward velocities of 20–100 km/s (Beckers 1972). Recently, the existence of more violent “type II” spicules is reported (De Pontieu et al. 2007b). The type I and II spicules are considered to have their on-disk counterparts of mottles (Roupe van der Voort et al. 2007) and the rapid blue-shifted events (RBES) (De Pontieu et al. 2009; Roupe van der Voort et al. 2009; McIntosh & De Pontieu 2009), respectively. The dynamic fibrils observed on the disk in active regions have maximum lengths of several Mm, lifetimes of 2–8 min, and maximum velocities of 10–40 km/s (Hansteen et al. 2006; De Pontieu et al. 2007a). Roupe van der Voort et al. (2007) reported that the dynamic fibrils are considered to be the active region counterpart of the quiet-sun mottles.

Theoretical studies have suggested various models for these chromospheric jets (see Sterling 2000, for a review). For the dynamic fibrils, the periodic acoustic wave model is in agreement with observations (Hansteen et al. 2006; De Pontieu et al. 2007a; Heggland et al. 2007), particularly in terms of the correlation between deceleration and maximum velocity. The origin of spicules (types I and II) is still under debate. Many candidates, such as acoustic waves (e.g., Hollweg 1982; Suematsu et al. 1982), Alfvén waves (e.g., Hollweg et al. 1982; Kudoh & Shibata 1999), and magnetic reconnection (e.g., Uchida 1969; Heggland et al. 2009; Takasao et al. 2013) have been suggested. Most of these models include a process by which the transition region is lifted by the shock wave propagating upward into the corona. This process is called the shock-transition region interaction (Hollweg 1982). Several multi-dimensional simulations with the sophisticated modeling of convective motion have been reported (Hansteen et al. 2006; Martínez-Sykora et al. 2009;

Hegglund et al. 2011). Although some of these studies is intended to be the representative for quiet regions, the simulated chromospheric jets was significantly shorter than the observed spicules.

Using idealized one-dimensional hydrodynamic simulations, Shibata & Suematsu (1982) explained why the spicules are long in the coronal hole. The key process is the amplification of the strength of the shock wave in the solar chromosphere. Based on their idea, we investigate the effect of the coronal temperature on the scale of the solar chromospheric jets using two-dimensional magnetohydrodynamic simulations with more realistic physical processes, to provide a unified perspective on the quiet region spicules, the coronal hole spicules, and the active region dynamic fibrils.

## 2. Numerical Model

We develop a new radiation magnetohydrodynamic code for the dynamical modeling of the solar atmosphere. The equations solved by this code include gravity, a LTE equation of state, the radiative cooling, and thermal conduction along the magnetic field line.

The solar atmosphere is filled with strong shock waves with a wide range of plasma beta. A robust numerical scheme is required for the simulation of these regions. We employ a higher-order magnetohydrodynamic scheme based on the constrained transport method (Evans & Hawley 1988) with divergence-free magnetic field reconstruction (Balsara 2009). The equations are solved in the conservative form. We do not consider explicit viscosity or magnetic diffusivity.

We assume the local thermodynamic equilibrium for the equation of state. The six most abundant elements are accounted with the metal mass fraction of Asplund et al. (2006). The formation of molecular hydrogen is not considered.

The radiative cooling term is evaluated as a combination of the two different approximations. In the photosphere and lower chromosphere, the radiative transfer equation is solved directly for the better modeling of the convective motion (Nordlund 1982). The short characteristic method (Kunasz & Auer 1988) is employed with the A4 quadrature in Carlson (1963). The gray approximation is assumed with the OPAL Rosseland mean opacity (Iglesias & Rogers 1996) in the high-temperature region and the opacity of Ferguson et al. (2005) in the low-temperature region. In the upper chromosphere and corona, the optically thin radiative loss function is employed to estimate the radiative cooling. The loss function is calculated from the CHIANTI atomic database (Landi et al. 2012), with the extension by Goodman & Judge (2012) for the chromospheric temperature. These photospheric and chromospheric cooling terms are switched by the function of the column mass density. In addition to these terms, we include an artificial heating term which becomes active only when the temperature falls below 2,500 K.

Spitzer-type anisotropic thermal conduction is treated by second-order operator splitting and the second-order super-time-stepping method (Meyer et al. 2012). The flux-limiting method (Sharma & Hammett 2007) is employed to maintain the monotonicity of the temperature.

The two-dimensional numerical domain in the  $XZ$ -plane extends from 2 Mm below the surface to 14 Mm above. The horizontal extent is 18 Mm. The uniform grid size is 42 km in the horizontal direction and 32 km in the vertical direction.

The bottom boundary condition is the “open” boundary. The total (gas plus magnetic) pressure equilibrium is assumed. The entropy of the upward plasma is fixed. The upward velocity field is slowly damped to the horizontally uniform upflow which complements the mass flux by the downward flow (e.g., Bercik 2002). This weak damping is not important in the present results but able to suppress the unrealistic instability which appears after

the long time integration. The downward plasma evolves adiabatically and freely. The top boundary has a free-slip condition and is open for vertical flow. The density is extrapolated exponentially by the scale height at the boundary. Our two-dimensional simulation with a top boundary at the lower corona cannot maintain the 1 MK coronal temperature (e.g., Leenaarts et al. 2011; Heggland et al. 2011). To prevent the corona from being cooled by radiation and thermal conduction, the conductive flux is introduced through the top boundary to heat the corona. In this study, the conductive flux is adjusted to preserve the different coronal temperature at the top boundary,  $T_c$ . The magnetic field is assumed to be vertical at the top and bottom boundaries. The periodic boundary condition is employed horizontally.

The initial condition is the plane-parallel atmosphere with a uniform vertical magnetic field of 3 G. The sufficiently relaxed convection is obtained after the integration of 5 solar hours with a temperature at the top boundary,  $T_c$ , of 1 MK. We impose the uniform vertical magnetic field of 30 G on the relaxed atmosphere and integrate another 3 solar hours with the same  $T_c$ . Next, we change the temperature at the top boundary,  $T_c$ , to 2, 1, and 0.4 MK to imitate the conditions of the active region, the quiet region, and the coronal hole, respectively. The simulations are integrated for another 1 solar hour after the change of  $T_c$ . We find that the coronal density and temperature reach statistical equilibrium within 20 min. The data analyzed below is the last 30 min of each simulation.

### 3. Results

Figure 1 shows snapshots from three simulations with the temperature at the top boundary,  $T_c$ , set to 2, 1, and 0.4 MK. We find the strong magnetic field concentration near  $X = 8$  Mm. Because the magnetic field structure is essentially the same among these three simulations, we can concentrate on the effect of the coronal temperature. The

jet-like structures with various scales are formed in the chromosphere. These structures are basically driven by the shock waves, arising from convective motion, which pass through the transition region. This process is consistent with both the one-dimensional simulations (Hollweg et al. 1982; Suematsu et al. 1982) and multi-dimensional simulations (Hegglund et al. 2011). We clearly find that the simulation with a lower coronal temperature produces higher chromospheric jets. The density near the top of each jet and over the entire corona is smaller when  $T_c$  is lower. The widths of the produced jets in these simulations are approximately independent of  $T_c$  if measured at a specific height like  $Z = 3$  Mm, but the jets become sharper near their tops in the lower  $T_c$  simulations.

We automatically detect the chromospheric jets in the simulations for the purpose of quantitative comparison. The procedure is basically same as that in Hegglund et al. (2011). The vertical motion of the transition region along the magnetic field line is fitted by a parabola. The maximum length (i.e., the maximum height of transition region evaluated from the initial height), the lifetime, the maximum upward velocity, and the deceleration for each jet are calculated from the fitting. The result of the statistical analysis is shown in Figure 2. We find a clear correlation between maximum length and maximum upward velocity for all three simulations (panels (a)–(c)). The lifetime roughly correlates with the maximum velocity for each simulation (panels (d)–(f)). The lifetime becomes longer and the correlation between lifetime and maximum velocity becomes stronger when the coronal temperature is lower. The correlation between deceleration and maximum velocity is relatively weak (panels (g)–(i)). The deceleration for  $T_c = 2$  MK (panel (g)) is distributed over a relatively broad range, exceeding the gravitational deceleration on the solar surface. The deceleration for  $T_c = 0.4$  MK (panel (i)) is concentrated below the gravitational deceleration.

The abovementioned dependence on the temperature at the top boundary,  $T_c$ , can be

explained as follows. When  $T_c$  is high (i.e., 2 MK) and the chromospheric jets are small, as in panels (a), (d), and (g) in Figure 2, the obtained correlations are consistent with the “shock deceleration hypothesis” suggested by Heggland et al. (2007). According to this hypothesis, the deceleration is determined by the periodicity of the slow-mode shock wave and can exceed the gravitational deceleration (see Eq. (1) in Heggland et al. 2007). The lifetime of the jet is determined by the period of the driving shock wave. The dotted lines in panels (a), (d), and (g) are the theoretical lines of parabolic motion with lifetimes of 2, 3, and 5 min. These lines are well-consistent with the results from the simulation with  $T_c = 2$  MK. Because the lifetime of chromospheric jet is equal to the period of driving acoustic wave in the “shock deceleration hypothesis”, the long lifetime in  $T_c = 0.4$  MK case (panels (f)) requires long period of driving waves, which is not expected under the short acoustic cutoff period in the lower solar atmosphere (e.g. Michalitsanos 1973). The deceleration by the gravity becomes more important in this case. The resulting motion of taller chromospheric jets approaches free-fall. The dashed lines in panels (c), (f), and (i) indicate the theoretical lines of ballistic motion, which approximately explain the properties of simulated jets. Since the simulated jets in the case of  $T_c = 0.4$  MK do not exactly follow ballistic paths, both of the gravitational and gas pressure gradient forces play a role in addition to the inclination of the magnetic field line. The case of  $T_c = 1$  MK, shown in panels (b), (e), and (h), exhibits intermediate properties between these two extremes.

To consider the abovementioned view on the determination of deceleration, we investigate the vertical force near the top of the chromospheric jets. The vertical component



of the equation of motion can be written as follows.

$$\begin{aligned}
 -\frac{DV_z}{Dt} &= D_{\parallel}^G + D_{\parallel}^P + D_{\perp}^G + D_{\perp}^P + D_{\perp}^L \\
 D_{\parallel}^G &= g_0 b_z^2 \\
 D_{\parallel}^P &= \mathbf{b} \cdot \left( \frac{1}{\rho} \nabla P \right) b_z \\
 D_{\perp}^G &= g_0 - D_{\parallel}^G = g_0 b_x^2 \\
 D_{\perp}^P &= \frac{1}{\rho} \frac{\partial P}{\partial z} - D_{\parallel}^P \\
 D_{\perp}^L &= -\frac{1}{\rho} (\mathbf{J} \times \mathbf{B})_z
 \end{aligned} \tag{1}$$

Here,  $g_0$  is the gravitational acceleration at the solar surface,  $P$  is the gas pressure,  $\mathbf{B}$  is the magnetic flux density,  $\mathbf{J}$  is the current density,  $D/Dt = \partial/\partial t + \mathbf{V} \cdot \nabla$  is the Lagrangian derivative, and  $\mathbf{b} = \mathbf{B}/|\mathbf{B}|$  is a unit vector parallel to the magnetic field. If we assume that the transition region at the top of the chromospheric jets is the contact discontinuity, the deceleration of the jets can be approximated by  $-DV_z/Dt$  near the transition region. The result is shown in Figure 3. Panels (a)–(c) show the deceleration produced by the total force parallel to the magnetic field  $D_{\parallel}^P + D_{\parallel}^G$  versus the deceleration calculated by the motion of the chromospheric jets. Although there is some level of dispersion, the motion of the transition region is roughly explained by the forces parallel to the magnetic field. The possible candidates of the discrepancy are the effect of the forces perpendicular to the magnetic field ( $D_{\perp}^G$ ,  $D_{\perp}^P$ , and  $D_{\perp}^L$ ), the deviation of the transition region from the contact discontinuity by the thermal conduction and waves, and the fitting and discretization errors. Panels (d)–(f) show the deceleration produced by the gravity parallel to the magnetic field  $D_{\parallel}^G$ .  $D_{\parallel}^G$  is more concentrated near the value of gravitational acceleration in the lower coronal temperature. Because the structure of the magnetic field is nearly independent of the coronal temperature, the temperature dependence in these panels are caused by the difference of the height of produced jets. When the coronal temperature is higher, the maximum length of jets becomes small and the transition region moves near the root

of the magnetic field where the magnetic field is more inclined. Panels (g)–(i) show the deceleration produced by the gas pressure gradient force parallel to the magnetic field  $D_{\parallel}^P$ . In  $T_c = 0.4$  MK case, the pressure gradient force always decreases the deceleration of the jets. However, in  $T_c = 2$  and 1 MK cases, a part of the jets is decelerated by the pressure gradient force. This is consistent with the “shock deceleration hypothesis” where the deceleration is determined by the periodic shock wave.

To understand why the scale of the chromospheric jets depends on the coronal temperature, we investigate the relationship between the coronal gas pressure and the maximum velocity of the produced jets as shown in Figure 4. The scale height of the gas pressure in the corona is sufficiently long and the gas pressure is almost constant across the transition region. Thus, we can use the coronal gas pressure,  $P_c$ , as the representative value of the gas pressure near the transition region. Shibata & Suematsu (1982) suggest that the density difference at the transition region causes the differences in the amplitude of the chromospheric shock wave and in the size of the chromospheric jets. For a linear wave, the energy flux of the slow magneto-acoustic wave is conserved during the propagation as  $S\rho V^2 C_s = \text{constant}$ . Here  $S$  is the cross-section of the magnetic flux tube,  $C_s$  is the speed of the slow magneto-acoustic wave, and  $V$  is the velocity parallel to the magnetic field. This relation is reduced to  $V \propto (S\rho C_s)^{-1/2} \sim (SP_c)^{-1/2}$ . The dependence on  $S$  does not appear in our current results because the magnetic field structure is almost the same in each of our three simulations. In fact, the shock wave is strong in the upper chromosphere, and the energy dissipation near the shock front violates the energy flux conservation. Ôno et al. (1960) analytically derived the relation of  $V \propto P_c^{-0.236}$  for a strong shock wave with the constant chromospheric temperature and an adiabatic heat ratio of 5/3. Shibata & Suematsu (1982) reported the relation of  $V \propto P_c^{-0.23}$  in their one-dimensional adiabatic hydrodynamic simulation, which is very close to the analytic estimate for strong shock wave. We obtain the relation of  $V \propto P_c^{-0.089}$  from the three simulations with different

coronal temperatures. This result indicates that another energy-loss process contributes to the formation of chromospheric jets in our simulations. The possible candidates are the radiative energy loss, the energy leakage by multidimensional effects, the thermal conduction, and the latent heat of ionization. The shock-transition region interaction (Hollweg 1982) and the dynamic variation of the chromospheric temperature will also affect the result. We note that the amplitude of the maximum upward velocity depends only on the nonlinear propagation of acoustic waves in the photosphere and chromosphere and does not depend on the deceleration models discussed in the preceding paragraphs.

#### 4. Discussion

We can compare our three simulations with different temperatures at the top boundary ( $T_c = 2, 1,$  and  $0.4$  MK) to the observations of the active region dynamic fibrils, the quiet region spicules, and the coronal hole spicules, respectively. Panels (a), (d), and (g) in Figure 2 show behavior similar to the observation of the active region dynamic fibrils by De Pontieu et al. (2007a). The properties of the spicules in quiet regions and coronal holes were investigated by Zhang et al. (2012) and Pereira et al. (2012). Both studies reported that the spicules became longer in the coronal hole and shorter in the quiet region, which was consistent with our results. We note that the parabolic trajectory of jets in our study are consistent with the type I spicules but inconsistent with the type II spicules, which exhibit linear trajectory. Because the top of the spicule was considerably affected by the observed wavelength (Pereira et al. 2014; Skogsrud et al. 2015), further studies are required for the more quantitative comparison. We also note that  $T_c = 0.4$  MK is too low for coronal holes and  $T_c = 2$  MK is also too low for active regions. The regional difference of density and the spatial inhomogeneity of temperature and density will explain at least a part of this discrepancy. The magnetic field strength is also not the typical value for these

regions. However, if the chromospheric jets are driven by the acoustic waves from the lower atmosphere, we expect that the magnetic field does not affect the scale of the jets strongly.

The numerical setting of the two-dimensional simulation by Heggland et al. (2011) was very similar to that in our study. The simulation with  $T_c = 1$  MK is consistent with Case B in their study. Their simulation employed the Bifrost code (Gudiksen et al. 2011) with more sophisticated treatment of radiation. This agreement supports the validity of our simulations. Martínez-Sykora et al. (2009) investigated the chromospheric jets in three-dimensional domain with the emerging magnetic flux. The typical length of their jets was approximately 1 Mm. The high coronal temperature produced by the energy release of the flux emergence, in addition to the rapid expansion of the magnetic field lines in the corona, is a possible explanation for why these jets were small.

In this study, we neglect some physical processes which are important to the chromosphere, including non-equilibrium hydrogen ionization (Carlsson & Stein 2002), more sophisticated treatments of radiation (Hayek et al. 2010; Carlsson & Leenaarts 2012), and three-dimensionality. We believe that the qualitative picture is not affected. The dependence on the grid size is investigated and we find that the qualitative picture is not affected.

This work was supported by JSPS KAKENHI Grant Number 15H03640, “Joint Usage/Research Center for Interdisciplinary Large-scale Information Infrastructures”, “High Performance Computing Infrastructure”, and the Program for Leading Graduate Schools, MEXT, in Japan. Numerical computations were carried out on the Cray XC30 supercomputer at Center for Computational Astrophysics, National Astronomical Observatory of Japan. The page charge of this paper is supported by Center for Computational Astrophysics, National Astronomical Observatory of Japan.

## REFERENCES

- Asplund, M., Grevesse, N., & Sauval, A. J. 2006, *Communications in Asteroseismology*, 147, 76
- Balsara, D. S. 2009, *Journal of Computational Physics*, 228, 5040
- Beckers, J. M. 1972, *ARA&A*, 10, 73
- Bercik, D. J. 2002, PhD thesis, Michigan State University
- Carlson, B. 1963, *Methods in Computational Physics*, ed. B. Alder, S. Fernbach, & M. Rotenberg (New York: Academic), 1
- Carlsson, M., & Leenaarts, J. 2012, *A&A*, 539, A39
- Carlsson, M., & Stein, R. F. 2002, *ApJ*, 572, 626
- De Pontieu, B., Hansteen, V. H., Rouppe van der Voort, L., van Noort, M., & Carlsson, M. 2007a, *ApJ*, 655, 624
- De Pontieu, B., McIntosh, S. W., Hansteen, V. H., & Schrijver, C. J. 2009, *ApJ*, 701, L1
- De Pontieu, B., McIntosh, S., Hansteen, V. H., et al. 2007b, *PASJ*, 59, 655
- Evans, C. R., & Hawley, J. F. 1988, *The Astrophysical Journal*, 332, 659
- Ferguson, J. W., Alexander, D. R., Allard, F., et al. 2005, *ApJ*, 623, 585
- Goodman, M. L., & Judge, P. G. 2012, *ApJ*, 751, 75
- Gudiksen, B. V., Carlsson, M., Hansteen, V. H., et al. 2011, *A&A*, 531, A154
- Hansteen, V. H., De Pontieu, B., Rouppe van der Voort, L., van Noort, M., & Carlsson, M. 2006, *ApJ*, 647, L73

- Hayek, W., Asplund, M., Carlsson, M., et al. 2010, *A&A*, 517, A49
- Hegglund, L., De Pontieu, B., & Hansteen, V. H. 2007, *ApJ*, 666, 1277
- . 2009, *ApJ*, 702, 1
- Hegglund, L., Hansteen, V. H., De Pontieu, B., & Carlsson, M. 2011, *ApJ*, 743, 142
- Hollweg, J. V. 1982, *ApJ*, 257, 345
- Hollweg, J. V., Jackson, S., & Galloway, D. 1982, *Sol. Phys.*, 75, 35
- Iglesias, C. A., & Rogers, F. J. 1996, *ApJ*, 464, 943
- Kudoh, T., & Shibata, K. 1999, *ApJ*, 514, 493
- Kunasz, P., & Auer, L. H. 1988, *J. Quant. Spec. Radiat. Transf.*, 39, 67
- Landi, E., Del Zanna, G., Young, P. R., Dere, K. P., & Mason, H. E. 2012, *ApJ*, 744, 99
- Leenaarts, J., Carlsson, M., Hansteen, V., & Gudiksen, B. V. 2011, *A&A*, 530, A124
- Martínez-Sykora, J., Hansteen, V., De Pontieu, B., & Carlsson, M. 2009, *ApJ*, 701, 1569
- McIntosh, S. W., & De Pontieu, B. 2009, *ApJ*, 707, 524
- Meyer, C. D., Balsara, D. S., & Aslam, T. D. 2012, *MNRAS*, 422, 2102
- Michalitsanos, A. G. 1973, *Sol. Phys.*, 30, 47
- Nordlund, A. 1982, *A&A*, 107, 1
- Ôno, Y., Sakashita, S., & Yamazaki, H. 1960, *Progress of Theoretical Physics*, 23, 294
- Pereira, T. M. D., De Pontieu, B., & Carlsson, M. 2012, *ApJ*, 759, 18
- Pereira, T. M. D., De Pontieu, B., Carlsson, M., et al. 2014, *ApJ*, 792, L15

Roupe van der Voort, L., Leenaarts, J., de Pontieu, B., Carlsson, M., & Vissers, G. 2009, ApJ, 705, 272

Roupe van der Voort, L. H. M., De Pontieu, B., Hansteen, V. H., Carlsson, M., & van Noort, M. 2007, ApJ, 660, L169

Sharma, P., & Hammett, G. W. 2007, Journal of Computational Physics, 227, 123

Shibata, K., & Suematsu, Y. 1982, Sol. Phys., 78, 333

Skogsrud, H., Roupe van der Voort, L., De Pontieu, B., & Pereira, T. M. D. 2015, ApJ, 806, 170

Sterling, A. C. 2000, Sol. Phys., 196, 79

Suematsu, Y., Shibata, K., Neshikawa, T., & Kitai, R. 1982, Sol. Phys., 75, 99

Takasao, S., Isobe, H., & Shibata, K. 2013, PASJ, 65, 62

Uchida, Y. 1969, PASJ, 21, 128

Zhang, Y. Z., Shibata, K., Wang, J. X., et al. 2012, ApJ, 750, 16

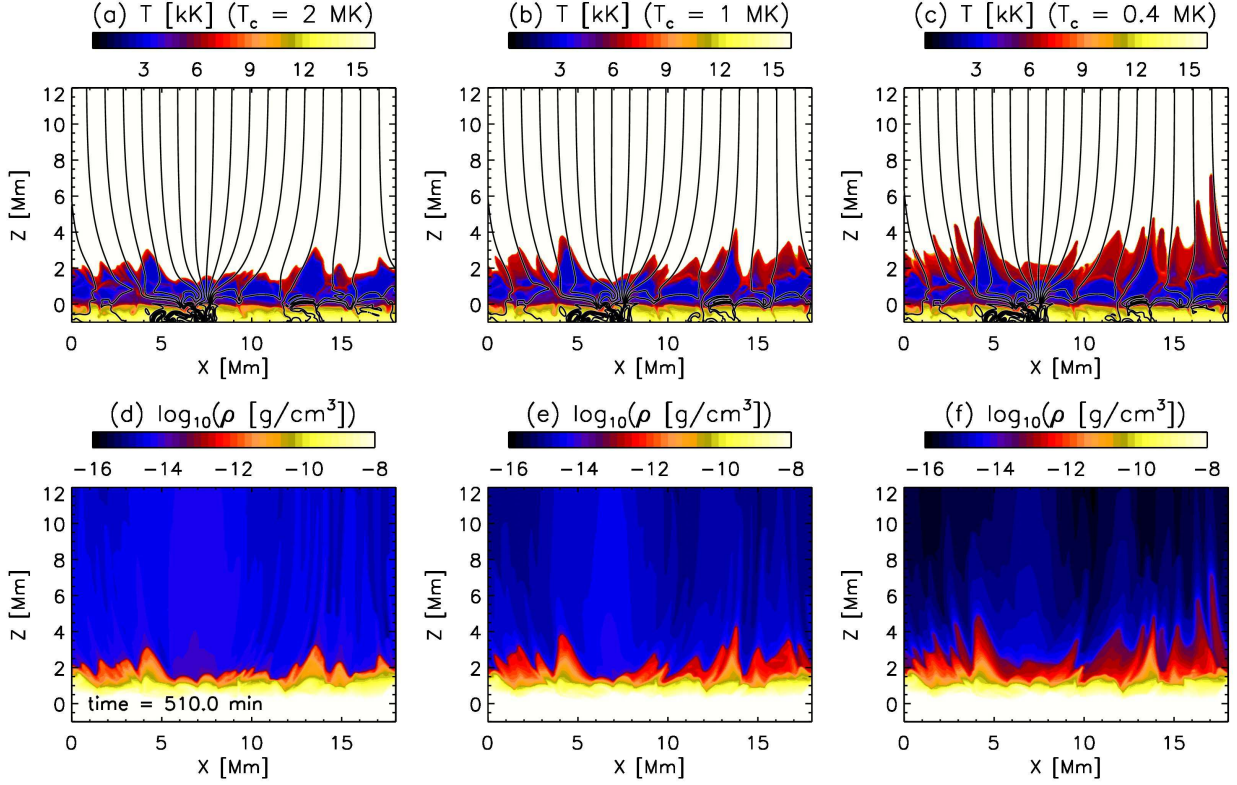


Fig. 1.— Snapshots from the three simulations with the different temperatures at the top boundary,  $T_c$ . Panels (a)–(c) show the temperature, and panels (d)–(f) represent the logarithm of mass density. The solid lines in panels (a)–(c) indicate the magnetic field lines. Panels (a) and (d) correspond to the simulation with  $T_c = 2$  MK, panels (b) and (e) correspond to the simulation with  $T_c = 1$  MK, and panels (c) and (f) correspond to the simulation with  $T_c = 0.4$  MK. (An animation of this figure is available in the electronic edition of *The Astrophysical Journal Letters*.)



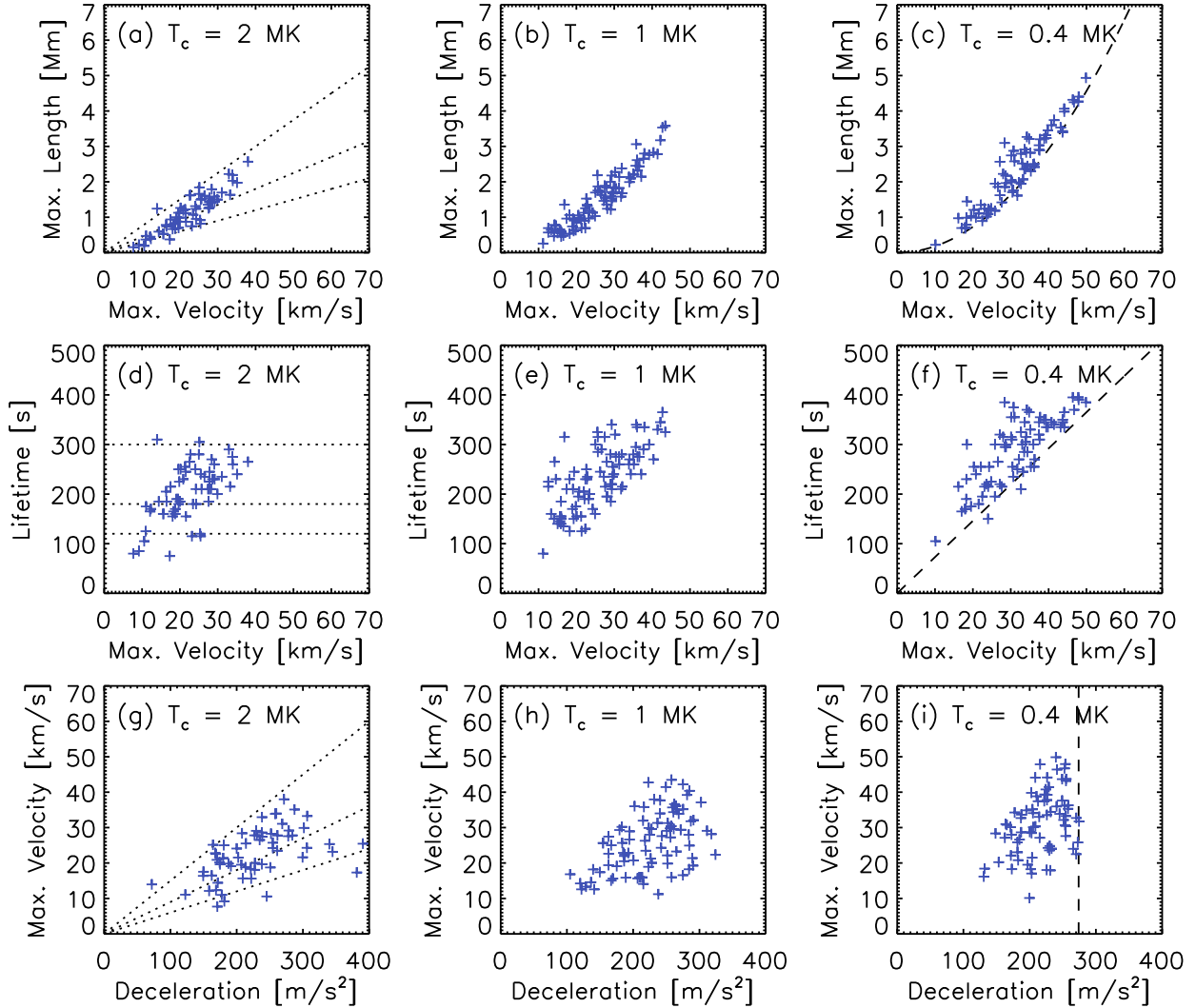


Fig. 2.— Statistical analysis of the produced chromospheric jets in the three simulations with different temperatures at the top boundary,  $T_c$ . Each cross sign corresponds to a chromospheric jet detected. See Section 3 for the description on the procedure for chromospheric jet detection. Panels (a), (d), and (g) correspond to  $T_c = 2$  MK, panels (b), (e), and (h) correspond to  $T_c = 1$  MK, and panels (c), (f), and (i) correspond to  $T_c = 0.4$  MK. The three dotted lines in panels (a), (d), and (g) represent the theoretical lines of parabolic motion with lifetimes of 2, 3, and 5 min. The dashed lines in panels (c), (f), and (i) indicate the theoretical lines of ballistic motion.

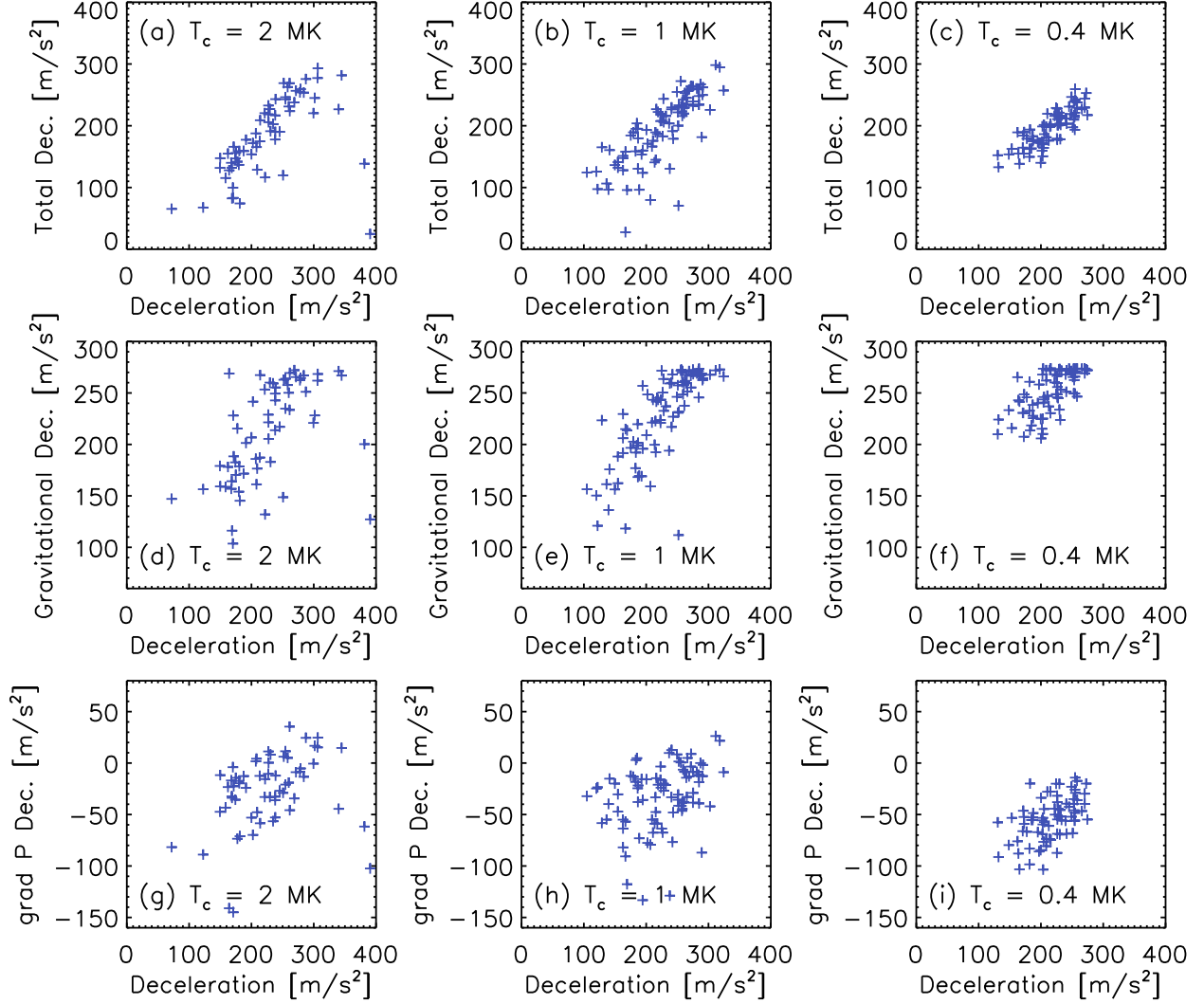


Fig. 3.— Contribution of gas pressure gradient and gravitational forces on the deceleration of the produced chromospheric jets in the three simulations with different temperatures at the top boundary,  $T_c$ . Each cross sign corresponds to a chromospheric jet detected. Panels (a), (d), and (g) correspond to  $T_c = 2$  MK, panels (b), (e), and (h) correspond to  $T_c = 1$  MK, and panels (c), (f), and (i) correspond to  $T_c = 0.4$  MK. See Section 3 for the description on the definition of each variables.

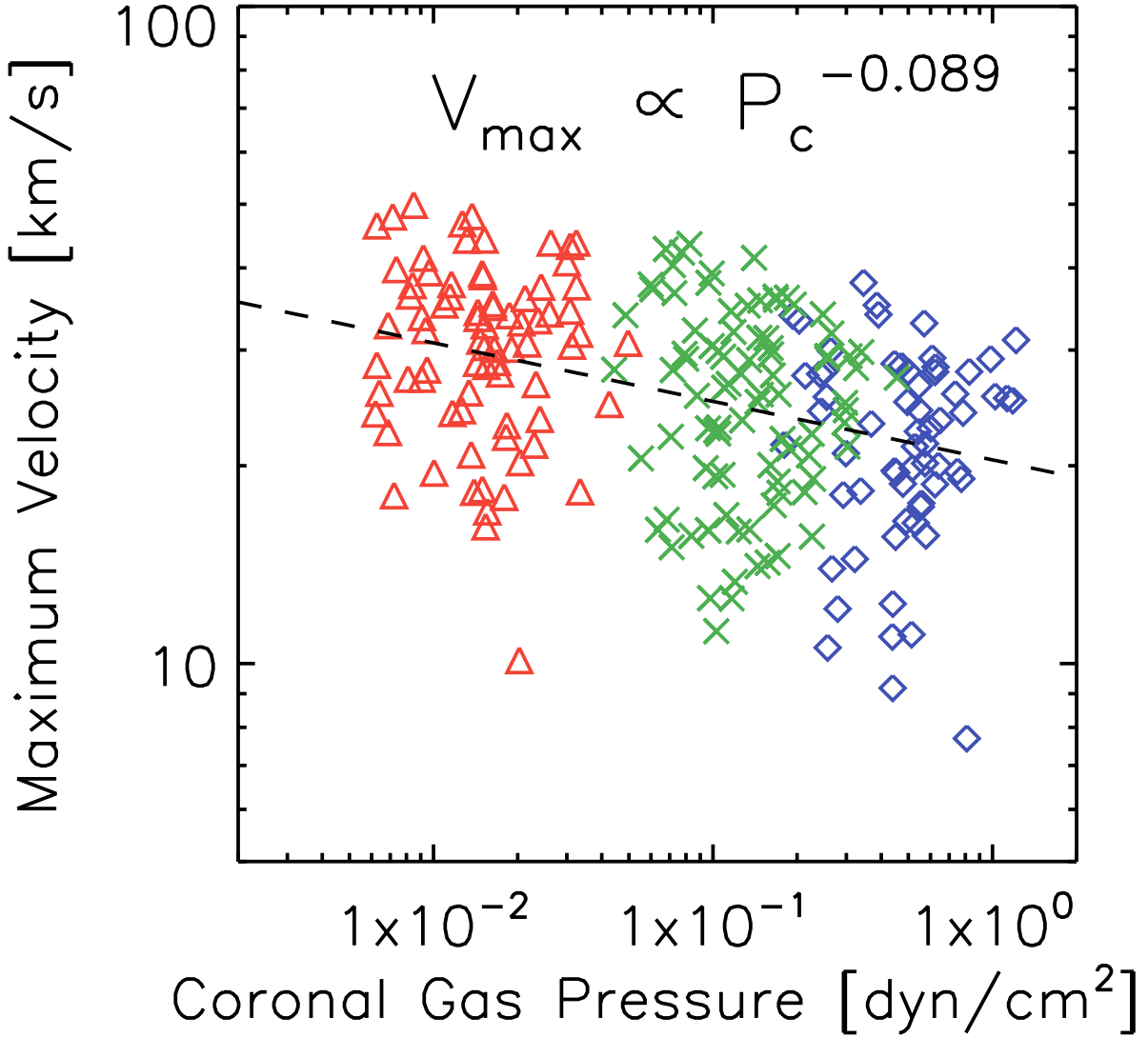


Fig. 4.— Dependence of the maximum upward velocity of the chromospheric jets on the coronal gas pressure from the simulation of  $T_c = 2$  MK (shown as blue diamonds),  $T_c = 1$  MK (shown as green crosses), and  $T_c = 0.4$  MK (shown as red triangle). The coronal gas pressure,  $P_c$ , is measured at the initial time of each chromospheric jet and averaged over the height range of 1–3 Mm above the transition region. The dashed line is the result of the least-square fitting,  $V_{\max} \propto P_c^{-0.089}$ , assuming a power-law relation.